Research Article

A Supporting Design Method When Longwall Face Strides across and Passes through a Roadway

Weidong Pan,[1,2] Xinyuan Li [1,2] YiWei Li,[1,2] Xiaobin Li [2] Qing Qiao,[3] and Haoran Gong[4]

[1]State Key Laboratory of Coal Resources and Safe Mining, China University of Mining and Technology-Beijing,
 Ding No. 11 Xueyuan Road, Haidian District, Beijing, China
[2]School of Energy and Mining Engineering, China University of Mining and Technology-Beijing, Ding No. 11 Xueyuan Road,
 Haidian District, Beijing, China
[3]School of Mechanics and Civil Engineering, China University of Mining and Technology-Beijing, Ding No. 11 Xueyuan Road,
 Haidian District, Beijing, China
[4]School of Emergency Management and Safety Engineering, China University of Mining and Technology-Beijing,
 Ding No. 11 Xueyuan Road, Haidian District, Beijing, China

Correspondence should be addressed to Xinyuan Li; lxy199521@student.cumtb.edu.cn

In coal underground mining, situation of longwall face striding across (SAR) or passing through roadway (PTR) is very common, especially in an inclined coal seam mining. A roadway supporting design method, consisting of a model using to determine the minimal rock strata thickness and a segmental supporting scheme, is developed. In addition, to represent the mechanical behaviour of the caved material authentically, an elastic model was developed. The results showed that the elastic model has a good agreement with the caved material mechanical behaviours at a relatively lower stress condition. By using a FDEM method, a real case in Xutuan coal mine is studied. Compared with the process without backfill, the z-displacement of cross-cut roof decreased shapely after backfilling, with a maximum z-displacement, decreases from 0.76 m to 0.13 m and from 0.39 m to 0.064 m in PTR and SAR section, respectively. Therefore, the possibility of fall of ground (FOG) and crushing accidents can be reduced effectively with backfilling material of wood cribs. And the maximum subsidence (SAR section side) of face floor is 0.16 m, which is small enough to ensure normal production. The results of this study are likely to be useful as a reference for the safe and efficient mining of coal resources under similar conditions.

1. Introduction

In underground coal mining, many roadways are excavated in coal or rock strata at different depths. Each of them plays a functional role in the coal mine production; a few are used for transportation while others are used for ventilation. Collectively, these roadways constitute a complex system. In the longwall mining field practice, it is common to encounter a situation in which roadways are laid ahead or below the longwall face [1–3], in particular, in the inclined coal seam mining. As the mining activity proceeds, it is inevitable for the longwall face to stride across (SAR) or pass though roadways (PTR). In China, particularly, owing to the large demand of coal consumption, this situation is more

common. This imposes a significant safety challenge on the mining activity, e.g., with respect to the stability of the roadway surrounding rock and the possibility of the fall of ground (FOG).

Much research has been done on SAR and PTR. Regarding SAR, when a longwall face is far away from a roadway in the advancing direction, the roadway is in a stable state. With the advance of the longwall face, the abutment pressure starts to increase [4]. The abutment pressure, together with the coal seam gravity, is transmitted to the face floor, which could increase the stress to several-fold above that of the primary rock and thus can affect the face floor and supporting structures. The mining-induced redistribution of the stress field leads to the initiation and

growth of preexisting cracks [5], leading to the formation of a face floor failure area. Thus, maximal floor failure depth plays a vital role in SAR. Once the maximal floor failure depth exceeds its critical value, the roadway is destroyed and the supports of the longwall face fall down. In addition, the roadway loosening zone cannot be ignored. After the roadway excavation, the stress in the surrounding rock becomes concentrated [6], which may exceed the bearing capacity of the surrounding rock and may damage the surrounding rock [7]. Therefore, the maximal floor failure depth and roadway loosening zone affect SAR. Regarding PTR, as the longwall face advances toward the roadway, the roof's hanging length increases gradually. When the hanging length reaches its critical value, the main roof breaks ahead of the longwall face, which sharply increases the load on the hydraulic supports and leads to the FOG and crushing of supports, especially when the longwall face suddenly advances into the roadway. In view of this, supporting schemes have been proposed to prevent possible accidents [2, 8], and these schemes provide guidelines and reference when doing supporting design for similar field conditions.

However, because of the inclination of the coal seam, it is inevitable to encounter a situation, in which both SAR and PTR appear simultaneously. Yet, little research was done to address these issues. In the work described in this paper, a mechanical model using to determine minimal rock strata thickness is proposed, and a segmental supporting scheme was introduced for different section of the roadway. Based on geological and mining condition of Xutuan coal mine, a FDEM numerical analysis is conducted by comparing the behaviour of the cross-cut rock mass with or without supporting.

2. Roadway Supporting Design Method

Figure 1 is an example of a longwall face striding across and passing through a roadway, simultaneously, because of the inclination of the coal seam. And there is a position where the rock strata, with a certain thickness, can hold the longwall face and the mining activity can carry out safely. Therefore, it is necessary to compute the minimal thickness of the rock strata. The calculation is guided by the realization that the rock strata at the minimal thickness should be able to support the weight of the longwall face equipment and should not collapse during the mining process.

2.1. Supporting Range Division. When the longwall face strides across a roadway, the thickness of the rock strata has three components, namely, the face floor failure depth (T_1), the bearing rock strata thickness (T_2), and the roadway broken height (T_3), as shown in Figure 2.

Owing to the existence of a bedding plane between the coal seam and the floor strata, the coal rib can be regarded as a deep foundation with a rough contact with plane OA [9]. Owing to the presence of unmined solid coal in the face-advancing direction, a half model compared with the model based on Terzaghi's principle [10] is established to deduce the longwall face failure depth T_1, as shown in Figure 3.
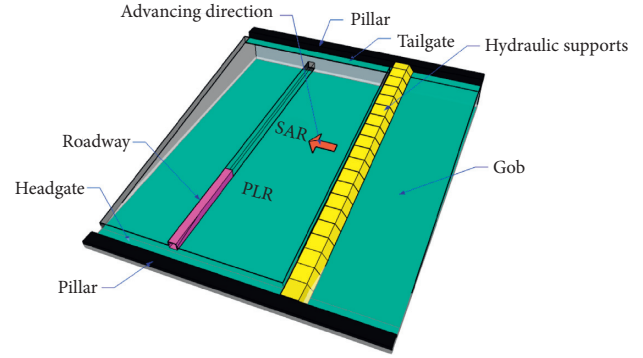

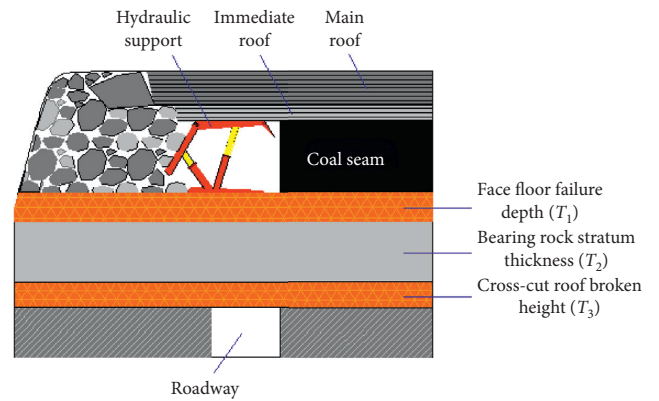Figure 1: Longwall face striding across and passing through a roadway.
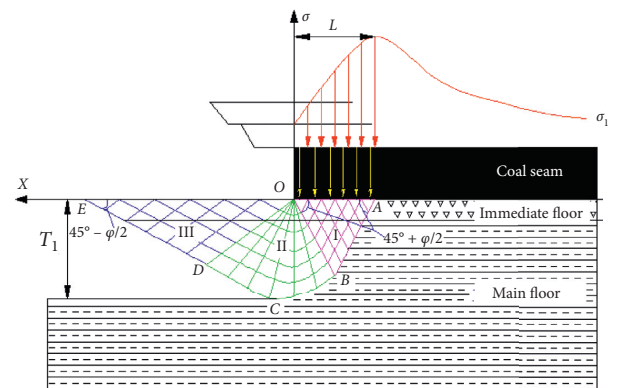

Figure 2: The components of rock strata.

Figure 3: Failure model of the 7# coal seam floor.

In the proposed model, under the coal rib, the floor is plastically deformed owing to the abutment pressure, and the rock mass forms a continuous slip surface. As shown in Figure 3, curve ACE represents the slip curve of the floor, where section BCD is a logarithmic spiral with B as the starting point. The plastic failure area of the floor is divided into three zones by the two radiation lines OB and OD: (1) the active stress area of zone I, (2) the transition area of zone II, and (3) the passive stress area of zone III. As shown in Figure 3, the failure depth T_1 is calculated as

$$T_1 = r\cos\theta = r_0 e^{\alpha\tan\varphi}\cos\theta,$$

$$\theta = \alpha - \frac{\pi}{4} + \frac{\varphi}{2}, \tag{1}$$

$$r_0 = \frac{L}{2\cos((\pi/4) + (\varphi/2))},$$

where r represents the distance between the logarithmic spiral and the original point (O); θ is the angle between the helical radius (r) and the vertical line; α is the angle between the waist line (OB) and the helical radius; r_0 is the waist length (OB) of the isosceles triangle OAB; φ is the inner-friction angle; and L is the distance between the peak abutment pressure and the longwall face. Hence,

$$T_1 = r_0 e^{\alpha\tan\varphi}\cos\left(\alpha - \frac{\pi}{4} + \frac{\varphi}{2}\right). \tag{2}$$

From the functional relationship, the value of T_1 is maximal when $(dT_1/d\alpha) = 0$. Thus,

$$\frac{dT_1}{d\alpha} = r_0 e^{\alpha\tan\varphi}\cos\left(\alpha - \frac{\pi}{4} + \frac{\varphi}{2}\right) - r_0 e^{\alpha\tan\varphi}\sin\left(\alpha - \frac{\pi}{4} + \frac{\varphi}{2}\right) = 0. \tag{3}$$

Then, T_1 can be estimated using the following equation:

$$T_1 = \frac{L\cos\varphi}{2\cos((\pi/4) + (\varphi/2))}e^{((\pi/4)+(\varphi/2))\tan\varphi}. \tag{4}$$

The bearing rock strata can be simplified as a clamped beam, as shown in Figure 4.

In Figure 4, L' is the width of the roadway; q is the pressure acted by the hydraulic support; and part of the strata weight above. The shear force and the bending moment at any point on the cross-section of the strata beam can be expressed as

$$F(x) = \frac{qL}{2}\left(1 - \frac{2x}{L'}\right),$$

$$M(x) = \frac{q}{12}\left(8L'x - 6x^2 - L'^2\right). \tag{5}$$

If the rock strata fractures in the shear form, the thickness of the strata (T_{2S}) becomes

$$T_{2S} = \frac{3F_{max}}{2R_s}, \tag{6}$$

where T_{2S} is the thickness of the rock strata when it fractures in the shear form, F_{max} is the maximal shear force the strata can withstand, and R_S is the shear strength.

If the rock strata fractures in the tensile form, the thickness of the strata (T_{2T}) becomes

$$T_{2T} = \sqrt{\frac{6M_{max}}{R_T}}, \tag{7}$$

where T_{2T} is the thickness of the rock strata when it fractures in the extension form, M_{max} is the maximal bending moment the strata can withstand, and R_T is the tensile strength.
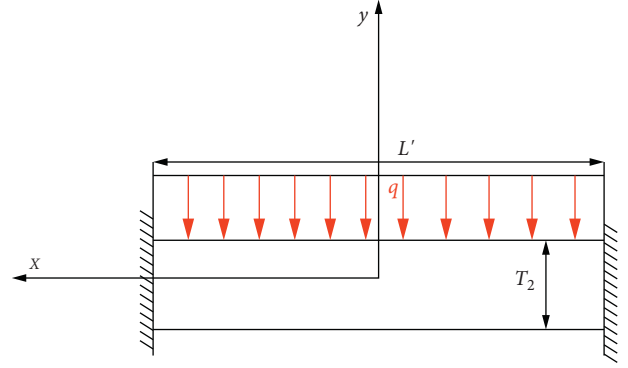

FIGURE 4: Clamped beam model.

The thickness of the bearing rock strata (T_2) should be larger than the minimal thickness of the strata to minimize the risk of shear or tensile fractures:

$$T_2 > \max(T_{2S}, T_{2T}). \tag{8}$$

After the excavation of the roadway, the stress in the surrounding rock starts to concentrate; eventually, the bearing capacity of the surrounding rock may be exceeded, damaging the surrounding rock [11]. The area of the damaged rock can be described by Protodjakonov's theory [12], which utilizes the values of the angle of the internal friction of the rock to characterize the rock mass. Such characterization of the area of the damaged rock is often adopted for the rock arch description, because it yields good results.

According to Protodjakonov's theory, a natural arch is formed above the roadway, and along this natural arch, the rocks may loosen or separate from the rock mass, as shown in Figure 5. The arch height can be determined by

$$T_3 = b = \frac{a}{f},$$

$$f = \frac{R_c}{10}. \tag{9}$$

Then, the minimal thickness of the rock strata can be calculated by

$$T = T_1 + T_2 + T_3. \tag{10}$$

And this thickness would be a boundary between backfilling section and no-backfilling section, beyond which the roadway needs no supporting measure.

2.2. Roadway Supporting Scheme. In this mining situation, it becomes imperative for normal production to design a reasonable supporting scheme to reinforce and support the roadway and prevent the subsidence of the longwall face, FOG, and support-crushing accidents. Since lower supporting cost, the backfilling technology, with waste rock, has been widely used in gob filling [13], which also have a great advantage in backfilling of SAR section.

As for PTR section, the longwall face at the PTR section passes through the roadway. During this process, the floor of the longwall face is hollow and the coal located in the roof of
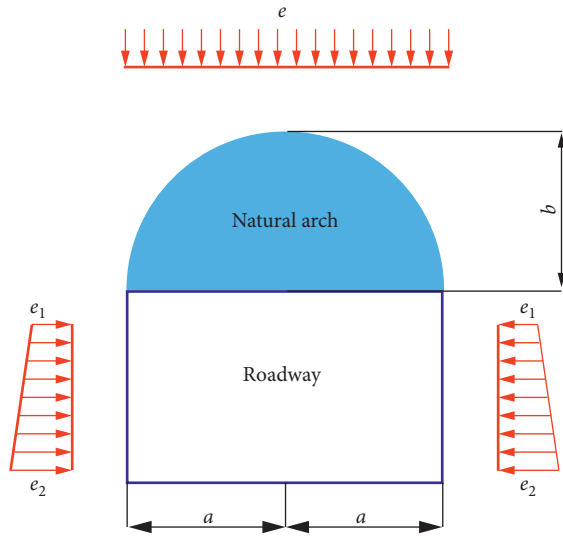
FIGURE 5: Natural arch theory model.

the roadway has a tendency to collapse and cave. Therefore, the main objective in this stage is to prevent the subsidence of the hydraulic support and provide enough supporting force to the roadway roof. Meanwhile, the support material cannot affect the production of the shearer. To improve the firmness of the face floor, concrete can be used to fill a certain height of the PTR section. Moreover, an intensive wood cribs should be laid previously and integrated with the concrete, which does not affect normal production, but provide supporting force to the roadway roof.

3. Case Study

3.1. Geological and Mining Condition. Xutuan coal mine, located at the Huaibei city, Anhui Province, China, was selected for a case study. In the Xutuan coal mine, No. 7 coal seam is one of the main minable seams and has a buried depth from 480 m to 510 m, with an average buried depth of 500 m. The vertical stress is 13.29 MPa, and the stress ratios are 0.43 and 0.21 in the advancing and inclined directions, respectively. No. 7 coal seam has a dip angle of 12°, thickness in the 4.0 m to 6.3 m range, with an average thickness of 5 m. The affiliated No. 7219 longwall face has an inclined length of 168 m and strike length of 420 m, and its succession face is No. 7229 longwall face. Moreover, there is a 100 m wide protective pillar between the two longwall faces, covering No. 7118 cross-cut. The cross-section of the cross-cut is rectangular, with 5 m width and 4.5 m height. The positions of the cross-cut and the longwall faces are shown in Figure 6.

The No. 7219 longwall face is a large mining height face with each of hydraulic shield supports weighing 36 t. Considering that the plan for moving the original face involved a long route with a significant amount of work, it was decided to extend the headgate and tailgate to the new stop line. As shown in Figure 6, No. 7219 longwall face continued to advance beyond the older stop line to the new stop line. In this way, additional coal resources could be recovered and the face-moving issue could also be resolved.

3.2. Supporting Design. The minimal thickness of the safety rock strata is the gap between the backfilling and non-backfilling of the SAR section. Based on field observations and measurements, the distance between the peak abutment pressure and the longwall face is 5 m (i.e., $L = 5$ m). The inner friction angle of the main floor was used because it is the median of the floor inner friction angle, as listed in Table 1. According on (4),

$$T_1 = 9.52 \, \text{m}. \tag{11}$$

The width of the No. 7118 cross-cut (L') is 5 m; the pressure acted by the hydraulic support and part of the strata weight above (q) is 0.51 MPa. The shear force ($F_{\max}$) reaches the maximal value at the position $x = \pm (L/2)$, and the maximal bending moment ($M_{\max}$) reaches the maximal value at the centre position of the strata ($x = 0$). According to (6) and (7), T_{2S} and T_{2T} are 0.15 m and 0.86 m, respectively. Thus,

$$T_2 = 0.86 \, \text{m}. \tag{12}$$

Based on the parameters in Table 1, the height of the natural arch can be calculated from (9), and the maximal cross-cut broken height (T_3) is

$$T_3 = 0.54 \, \text{m}. \tag{13}$$

Therefore, the minimal thickness of the safety rock strata can be determined by (10),

$$T = T_1 + T_2 + T_3 = 9.52 + 0.86 + 0.54 = 10.92 \, \text{m}. \tag{14}$$

According to the analysis above, the cross-cut can be sectioned using a rock strata thickness of 10.92 m. Therefore, the length of backfilling section is 52.5 m and PTR section are 30.5 m, as shown in Figure 7. Due to easy access, granular coal with radius in the 0.1–0.2 m range, corresponding to the field crashed coal dimensions, was used to backfill the roadway. And a concrete wall, with a thickness of 1 m, is built to prevent granular coal from flowing in SAR section near the backfilling material. In PTR section, the supporting material of concrete and wood cribs is used.

4. Numerical Model Construction

4.1. Global Model. In accordance with the geological characteristics of the coal measure strata, a numerical calculation model was established, as shown in Figure 8. The model dimensions were 200 m × 276 m × 150 m ($X \times Y \times Z$). In this model, three roadways, namely, the headgate, the tailgate, and the cross-cut, were excavated, and the cross-cut intersected with the headgate. The headgate and tailgate measured 4 m × 3 m ($Y \times Z$) and the cross-cut was rectangular (width, 5 m; height, 4.5 m). Around the panel, 50 m wide pillars were left to eliminate the boundary effect. To monitor displacement, three measure lines were set at the middle position of the walls and roof of the cross-cut, and the distance between every two measure points was 4 m.

FLAC3D was used for the numerical calculations. Atop the model, a vertical stress (13.286 MPa) was applied to
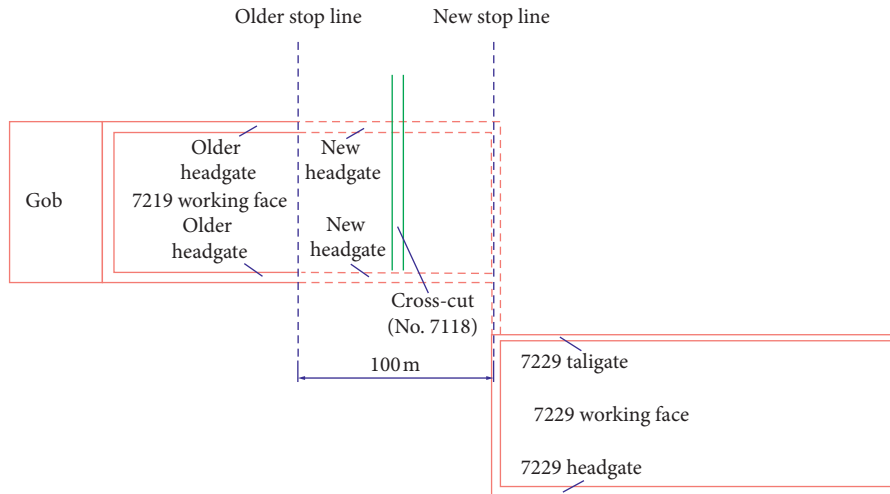
FIGURE 6: Positional relationship between the working faces and cross-cut.

TABLE 1: Physical and mechanical properties of main floor.

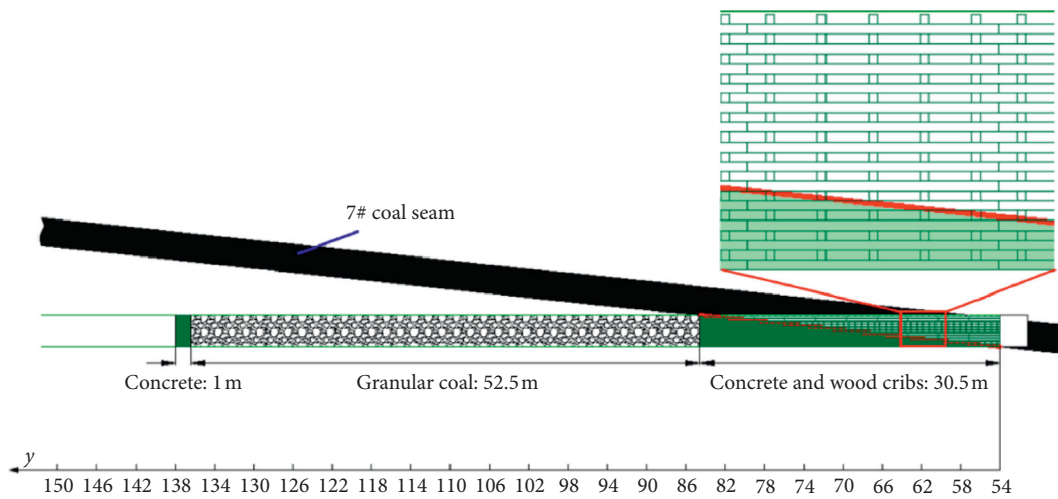| Lithology	Compressive strength (MPa)	Tensile strength (MPa)	Shear strength (MPa)	Inner friction angle (deg.)
Fine siltstone	45.9	9.0	13.0	35

FIGURE 7: No. 7118 cross-cut supporting design.

simulate the load applied by the overburden, and the bottom sides were roller-constrained. A horizontal stress was applied according to the in situ stress condition. Coal and rock, as an elastic-plastic medium [14], are suitable to modelling by the Mohr–Coulomb criterion. The Mohr–Coulomb criterion was used to simulate the rock and coal strata behaviours in this model.

Before this simulation, a laboratory test task was conducted to obtain the physical and mechanical properties of the surrounding rock. Much research has been conducted [15, 16], which validated that young modulus, cohesion, and tensile strength of the rock mass and coal seam are 0.1–0.25 times the laboratory result, and the Poisson ratio is 1.2–1.4 times the laboratory result. The parameters used in this model are listed in Table 2.

4.2. Elastic Model for Gob Modelling.

In the longwall mining method, the roof strata behind the longwall face are abandoned and collapse is allowed. When the face advances sufficiently far, the immediate roof behind it collapses at a distance that depends on the specific geological conditions. Failure of the roof continues until the roof and caved material come in contact. Under the load of the roof, the caved material is compacted gradually until the roof is balanced by the coal rib and the caved material. Thus, it is necessary to model the gob and its compaction [17]. The caved material does not behave as an intact rock; however, its stiffness varies with the stress to which it is subjected. In fact, it also exhibits certain strain-hardening characteristics.

The stress-strain behaviour of the caved material can be described by [18, 19], which were suggested for backfill materials by Salamon [20]:
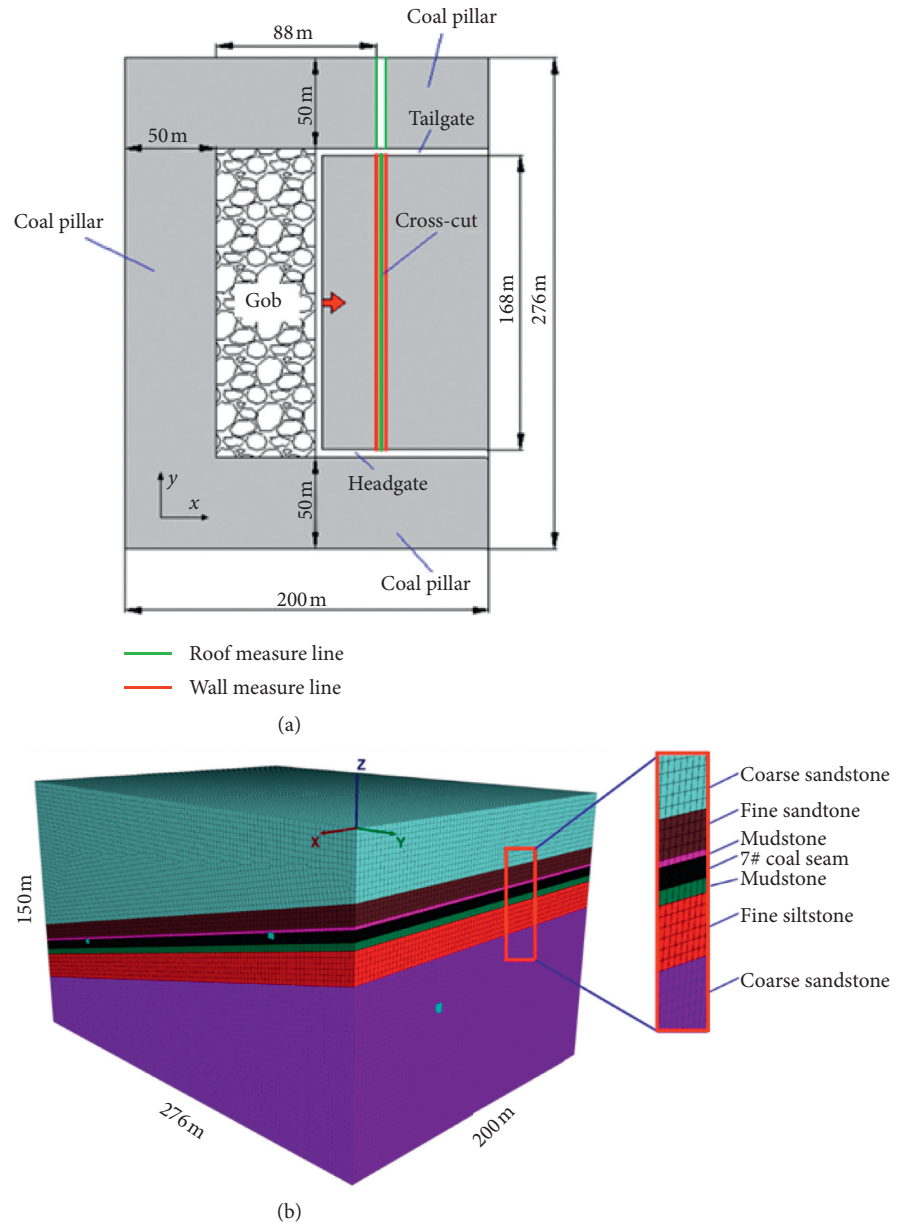
(a)

(b)

FIGURE 8: Numerical model configuration and measure line layout.

TABLE 2: Coal-rock layers and mechanical parameters used in the numerical model.

Rock strata	Thickness (m)	Density (kg/m³)	Bulk modulus (GPa)	Shear modulus (GPa)	Friction angle (deg.)	Cohesion (MPa)	Tensile strength (MPa)
Coarse sandstone	30.0–86.5	2580	10.3	8.4	37	4.3	5.9
Fine sandstone	9.0	2650	7.4	4.8	38	2.2	1.5
Mudstone	1.5	2540	2.3	1.2	27	1.2	0.8
7# coal seam	5.0	1400	0.3	0.12	18	0.3	0.15
Mudstone	3.4	2420	2.4	1.3	32	1.1	1.2
Fine siltstone	14.6	2500	3.0	1.9	35	2.4	4.3
Coarse sandstone	30.0–86.5	2660	8.1	4.9	37	2.8	2.2

$$\sigma = \frac{E_0 \varepsilon}{1 - (\varepsilon/\varepsilon_m)}, \quad (15)$$

$$\varepsilon_m = \frac{b-1}{b}, \quad (16)$$

$$E_0 = \frac{10.39\sigma_c^{1.042}}{b^{7.7}}, \quad (17)$$

where σ is the uniaxial stress applied to the material, ε is the strain under the applied stress, E_0 is the initial tangent modulus, ε_m is the maximal possible strain of the bulk rock material, b is the initial bulk factor, and σ_c is the compressive strength of the rock.

Behind the longwall face, the strata bends downward and breaks into different-size blocks until the lowest uncaved strata receives the support of the caved and bulk rock pile [19]. Therefore, the initial bulk factor b is closely related to the caving height and can be calculated as

$$b = \frac{H_c + h}{H_c}, \quad (18)$$

where H_c is the caving height and h is the mining height.

The caving height can be predicted by the following empirical criterion [21], which is consistent with field statistics of 4–11 times the thickness of the coal seam height [22]:

$$H_c = \frac{100h}{c_1 h + c_2}, \quad (19)$$

where c_1 and c_2 are coefficients that depend on the strata lithology, as shown in Table 3 [21, 23].

According to (15)–(19), the height of the roof caving zone H_c, the initial bulk factor b, the maximal strain ε_m, and the initial gob modulus E_0 are calculated (Table 4). The stress-strain behaviour of Salamon's model is shown in Figure 9 (blue line). The behaviour is approximately linear for stresses under 20 MPa, and it is exponential for higher stress values. This suggests that the caved material behaves like an elastic material for low stress values. As the objective of the present work was to analyse the deformability of the cross-cut (rather than observe failed zones), and because these material properties may change the stress level well behind the advancing longwall face rather than in front of the advancing longwall face, it is reasonable to assume elastic material properties in simulations of the caved material. An important practical advantage of using an elastic global model is computational efficiency, which allows to conduct a large number of analysis and parametric evaluations [24]. Kose and Cebi [25] suggested that the deformation modulus of the gob material ranges from 15 MPa to 3500 MPa, whereas, based on experiments, Shabanimashcool and Li [26] suggested that the deformation modulus of the caved material ranges from 60 MPa to 100 MPa. Jiang et al. [27] used a somewhat stiffer gob material with the deformation modulus and Poisson's ratio of 190 MPa and 0.25, respectively. To generate reasonable input parameters for the elastic model, a test material, with dimensions of $1\,m \times 1\,m \times 1\,m$, was simulated using FLAC3D. Loading was simulated by applying a velocity to the top surface; the parameters are listed in Table 5. The system's stress-strain behaviour was recorded and is shown in Figure 9 (red line).

As shown in Figure 9, the elastic model satisfactorily captures the caved material for stresses under 20 MPa. In practice, the stress behind the longwall face increases gradually with time. However, the stress cannot return to the original magnitude within a short-term period. In addition, the maximal in situ stress around the panel is 16 MPa, which is less than the limiting value of 20 MPa.

4.3. Supporting Material Modelling. Discrete Element Method (DEM) method has been used to simulation the behaviour of granular materials for a long time [28, 29]. In this paper, the granular coal, with the radius in the 0.1–0.2 m range, is used as the backfilling material. It is described as a cloud of discrete balls that were coupled to the FLAC3D continuous model via the "wall" medium, and this method is referred to as FDEM method. A uniform distribution model was used to represent the real distribution of the backfilling material of coal. Some parameters, including normal stiffness, shear stiffness, and friction coefficient, that were used here to model the granular coal were taken from literature [30]. Table 6 lists the parameters of the granular coal in our discrete model.

Three types of materials constitute the cross-cut supporting: concrete, wood, and granular coal. In this study, concrete was considered as a Mohr–Coulomb material [31]. Wood was simplified as an elastic material, although its actual mechanical behaviour is more complex [32]. However, the function of wood is just to support the cross-cut roof, and it only weakly affects the entire project. The parameters of the concrete and the wood cribs are listed in Table 7.

5. Simulation Results and Discussion

5.1. Cross-Cut Deformation during the Longwall Face Advancement. During the longwall face advancement, the stress around the cross-cut is disturbed. Subjected to the advancing abutment pressure, the walls and the roof of the cross-cut exhibit shape distortions in the form of displacement. The displacement of the surrounding rock was registered to obtain the displacement distribution.

5.1.1. SAR Section Deformation. As shown in Figure 10(a), when the longwall face advances, the distance between the longwall face and the cross-cut decreases (x-direction). The z-displacement of the cross-cut roof increases and then decreases, subjected to the advancing abutment pressure. However, the displacement along the cross-cut is different, owing to the thickness of the rock strata between the longwall face floor and the cross-cut roof, and the magnitude of the advancing abutment pressure. The z-displacement gradually increases with the advancement of the longwall face and as the advancing abutment pressure increases. However, the z-displacement begins to decrease when the longwall face advances 68–84 m, and the amount of reduction varies across the different

TABLE 3: Coefficients for average height of caving zone.

Strata lithology	Compressive strength (σ_c, MPa)	Coefficients	
		c_1	c_2
Strong and hard	>40	2.1	16
Medium strong	20–40	4.7	19
Soft and weak	<20	6.2	32

TABLE 4: Parameters for Salamon's model.

H_c (m)	B	ε_m	E_0 (MPa)
14.88	1.34	0.25	55.9
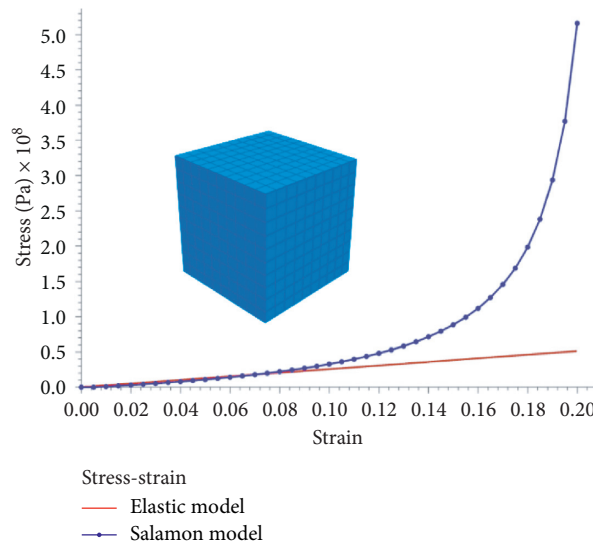
FIGURE 9: Stress-strain behaviour of caved material in gob.

TABLE 5: Parameters used in the elastic model for caved material.

Density (kg/m^3)	Young's modulus (MPa)	Poisson's ratio
1848	256.4	0.2

measured points. The maximal z-displacement decreases from 0.39 m to 0.064 m after backfilling. Moreover, as shown in Figure 10(b), the rate of change in the z-displacement gradually stabilizes when the y-coordinate is larger than 130 (the corresponding rock strata thickness is 9.78 m), which agrees with the calculation using the proposed model.

In Figure 11, after backfilling, the backfilling material interacts with the surrounding rock whenever a displacement occurs in any direction. Compared with the maximal x-displacement without backfilling, the maximal x-displacement decreases from 0.1 m to 0.03 m.

5.1.2. PTR Section Deformation. Several curves showing the variation of the z-displacement of the cross-cut roof when the longwall face advances were obtained and are shown in

Figure 12(a). When the longwall face advances, the distance between the longwall face and the cross-cut decreases (x-direction). The displacement along the z-direction of the cross-cut roof increases, subjected to the advancing abutment pressure. However, the displacement along the cross-cut is different, owing to the different thickness of the backfilling material and the magnitude of the advancing abutment pressure. The z-displacement gradually increases with the advancing longwall face and as the advancing abutment pressure increases. However, the z-displacement at the measured points $y = 74$, $y = 78$, and $y = 82$ starts to decrease, while that at the measured points $y = 54$, $y = 58$, $y = 62$, $y = 66$, and $y = 70$ continues to increase when the longwall face advances 68 m. The maximal z-displacement decreases from 0.76 m to 0.13 m after backfilling. In this way, the longwall face can pass through the cross-cut smoothly without worrying about the FOG and support-crushing accidents.

In Figure 13, after backfilling, the backfilling material and the surrounding rock are integrated with each other. Compared with the maximal x-displacement without

TABLE 6: Parameters for granular coal.

Radius (m)	Density (kg/m^3)	Normal stiffness (N/m)	Shear stiffness (N/m)	Friction coefficient	Cohesion (MPa)	Damp
0.1–0.2	1400	2×108	2×108	0.4	0	0.7

TABLE 7: Parameters for the concrete and the wood cribs.

Material	Constitutive model	Density (kg/m^3)	Young's modulus (GPa)	Poisson's ratio	Cohesive (MPa)	Friction angle (deg.)	Tension (MPa)
Concrete	Mohr-Coulomb	2400	30	0.2	3.18	55	1.43
Wood cribs	Elastic	364	4.3	0.38	—	—	—
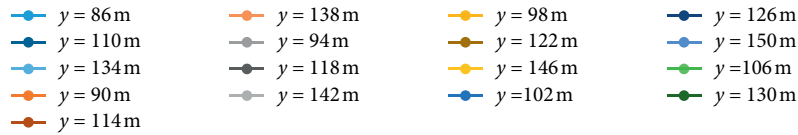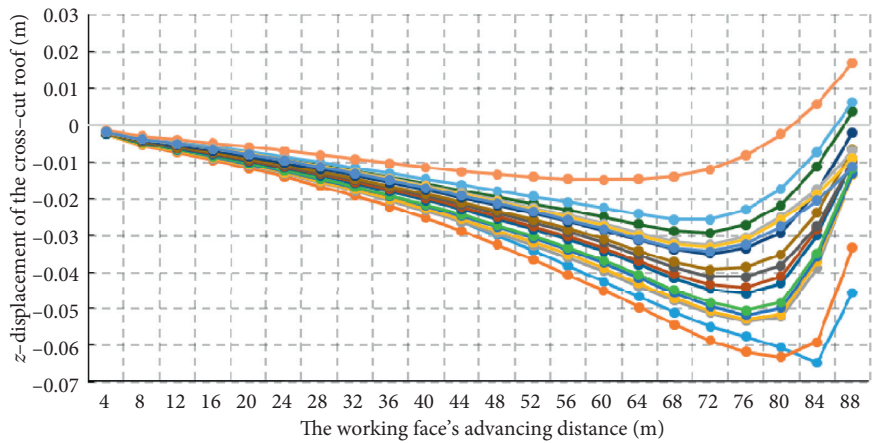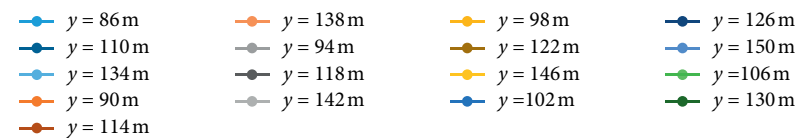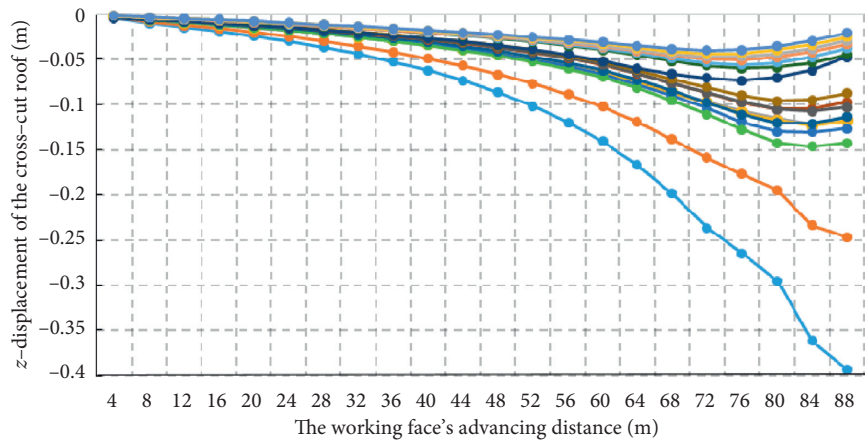
FIGURE 10: z-displacement of SAR section: (a) z-displacement of SAR section with backfilling and (b) z-displacement of SAR section without backfilling.
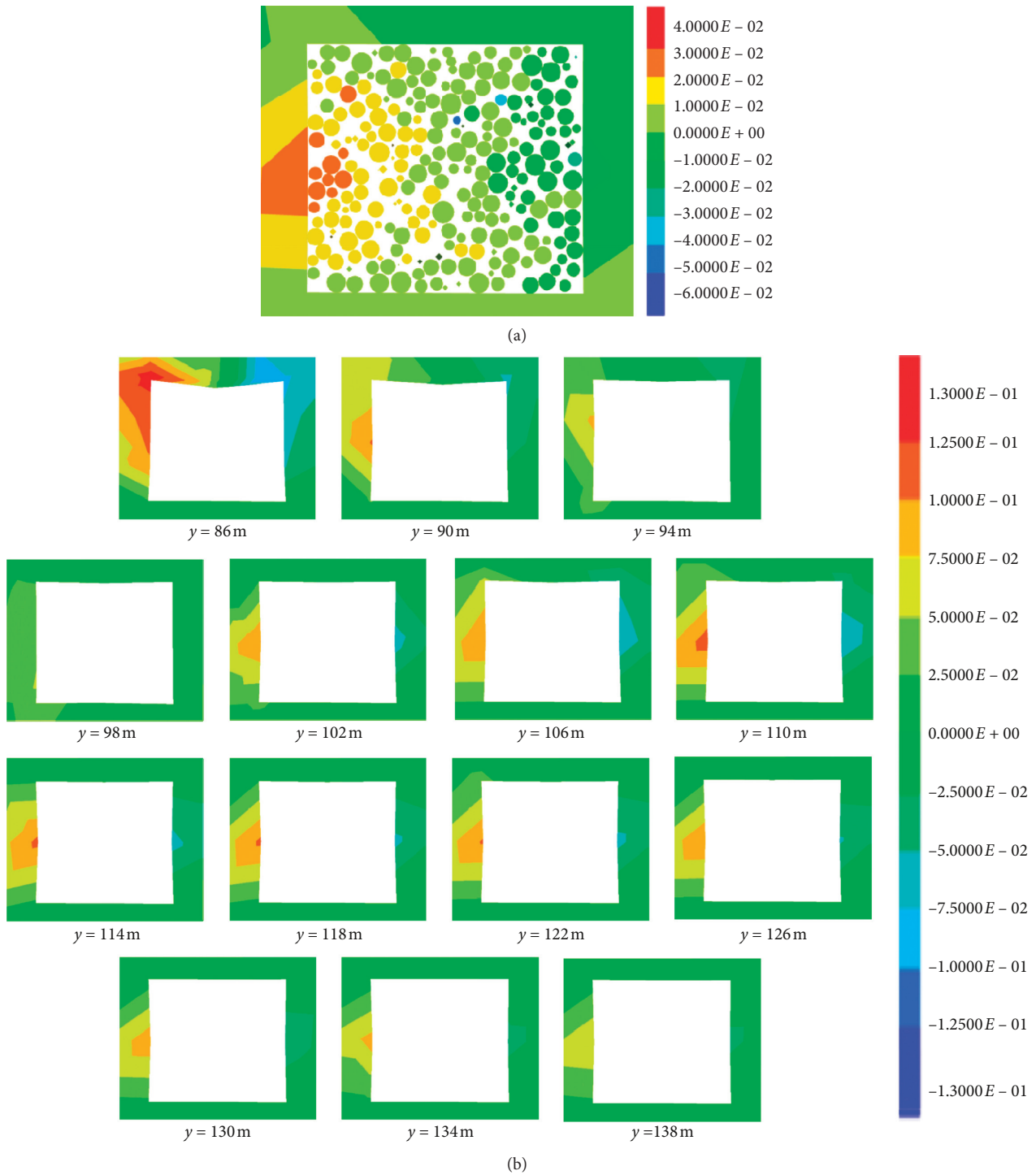
(a)

(b)

FIGURE 11: x-displacement of the cross-cut walls in SAR section. (a) Maximum x-displacement of the cross-cut walls after backfilling in measure point $y = 126$ m. (b) x-displacement of the cross-cut walls without backfilling.

backfilling, the maximal x-displacement decreases from 0.4 m to 0.014 m, which indicates that the wood cribs are stable and the rib spalling can be avoided. Thus, the normal production of the longwall face is guaranteed.

5.2. Face Floor Subsidence (SAR Section Side) When the Longwall Face Is above the Cross-Cut. When the longwall face is above the cross-cut, the face floor subsides at a maximum value. As shown in Figure 14, along the
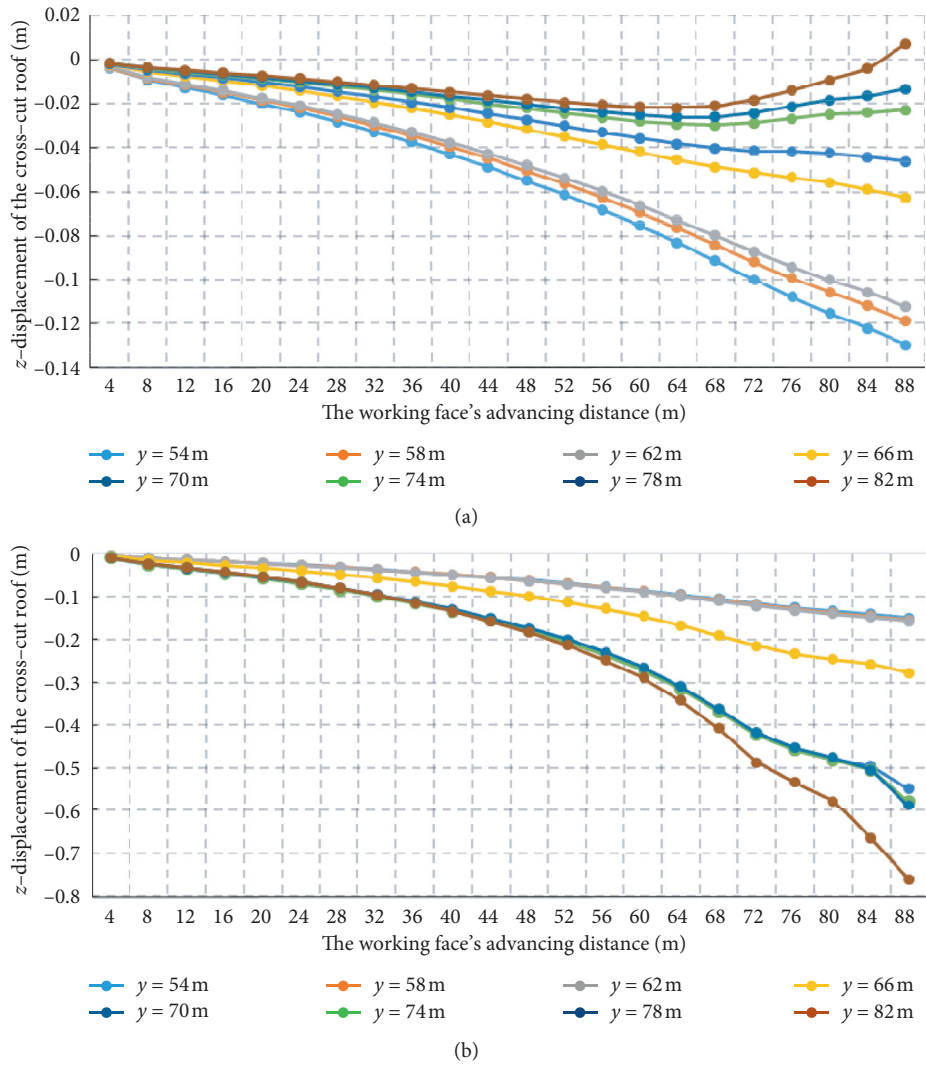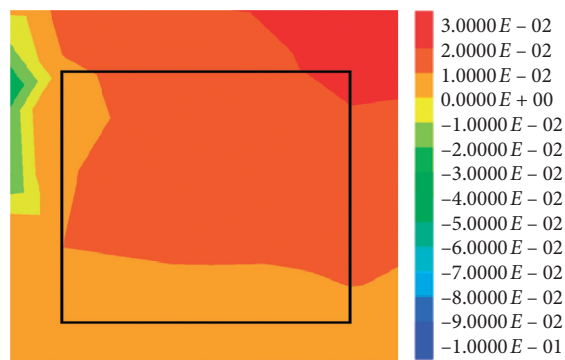
(a)

(b)

FIGURE 12: z-displacement of PTR section. (a) z-displacement of PTR section with backfilling. (b) z-displacement of PTR section without backfilling.
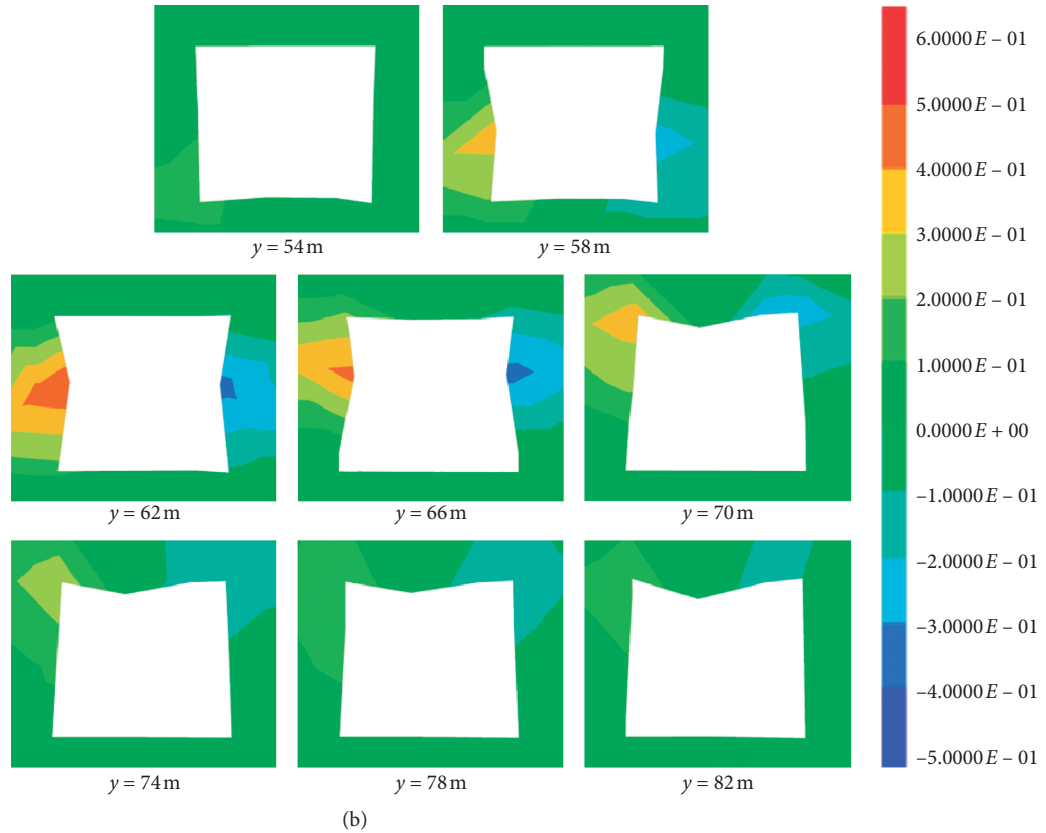

(a)

FIGURE 13: Continued.

(b)

FIGURE 13: x-displacement of the cross-cut walls in PTR section. (a) Maximum x-displacement of the cross-cut walls after backfilling in measure point $y = 70$ m. (b) x-displacement of the cross-cut walls without backfilling.

direction of the cross-cut axis, the magnitude of the subsidence decreases from 0.16 m to 0 m, then begins to increase in the opposite direction, and eventually stabilizes at 0.025 m. Note that the subsidence that occurs at the position y in the 132.5–140.5 m range is too small to affect normal production, for which the rock strata thickness is in an excellent agreement with the value calculated by the proposed model.

5.3. Effect of the Backfilling Material. The wood cribs and concrete, which are filled in PTR section as a backfilling material, provide support to the walls and the roof. The wood, which has a large Poisson's ratio, is a good material for maintaining the stability of the cross-cut, owing to its admirable Poisson effect and elastic deformability. The deformation of the PTR section is relatively larger than that of the SAR section. During the advancement of the longwall face, the displacement, either in the x-direction or in the z-direction, first increases and then decreases, because the peak advancing abutment pressure is at a certain distance in front of the longwall face. When a z-displacement occurs at the roof, the wood provides support to the roof and simultaneously generates lateral deformation, which provides support pressure to the walls. Meanwhile, the x-displacement that occurs at the walls provides confined

pressure to the backfilling material and increases its strength. In this way, both the FOG and the rib spalling can be controlled. As a soft material, the wood would not affect the shearer cutting coal, and the concrete would provide strong support to the supports and shearer when the longwall face passes through the cross-cut.

As an accessible material, the granular coal also exhibits a good performance in resisting deformation, and the continuity of displacements between the granular coal and rock mass indicates that the granular coal has a good displacement transmissibility, as shown in Figure 11(a). Subjected to the squeeze coming from the cross-cut deformation, the granular coal is compacted. The contact force between the coal and the cross-cut surface increases as the longwall face advances, especially in the middle of the walls (z-direction) and the roof (x-direction), as shown in Figure 15. However, this trend is interrupted when the face advances to 80 m; then, the contact force decreases as the face continues to advance. Note that the position of the peak contact force does not correspond to the field observations and measurements of the position of the advancing abutment pressure. The occurrence of this phenomenon may be related to excavation of the cross-cut, which may disturb the in-situ stress distribution and therefore would change the position of the advancing abutment pressure.
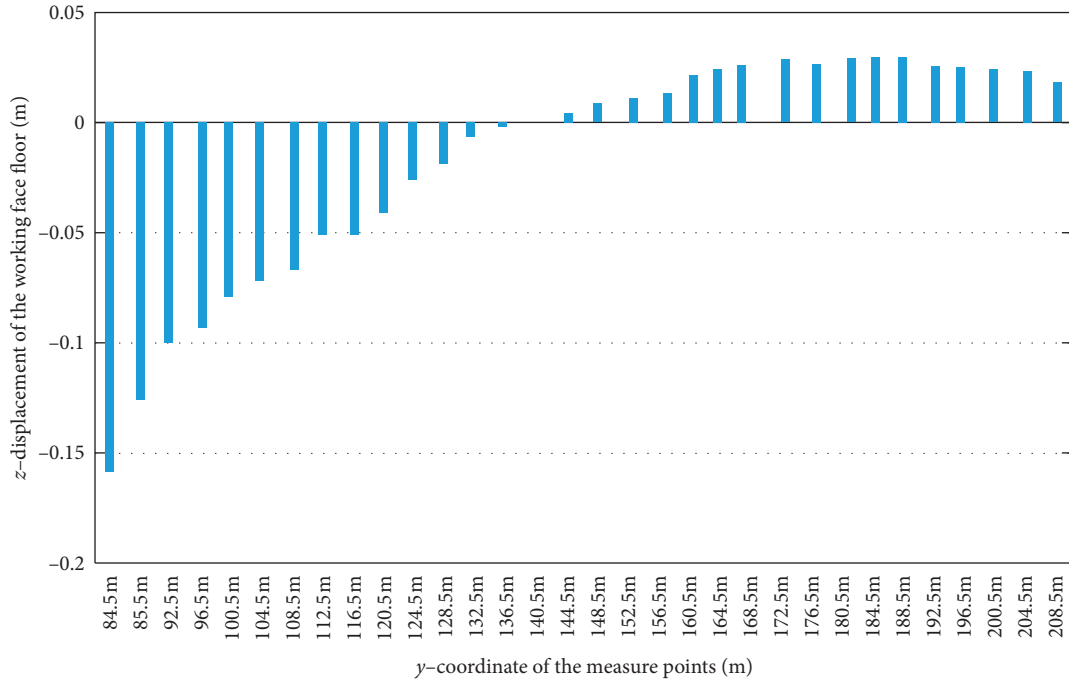
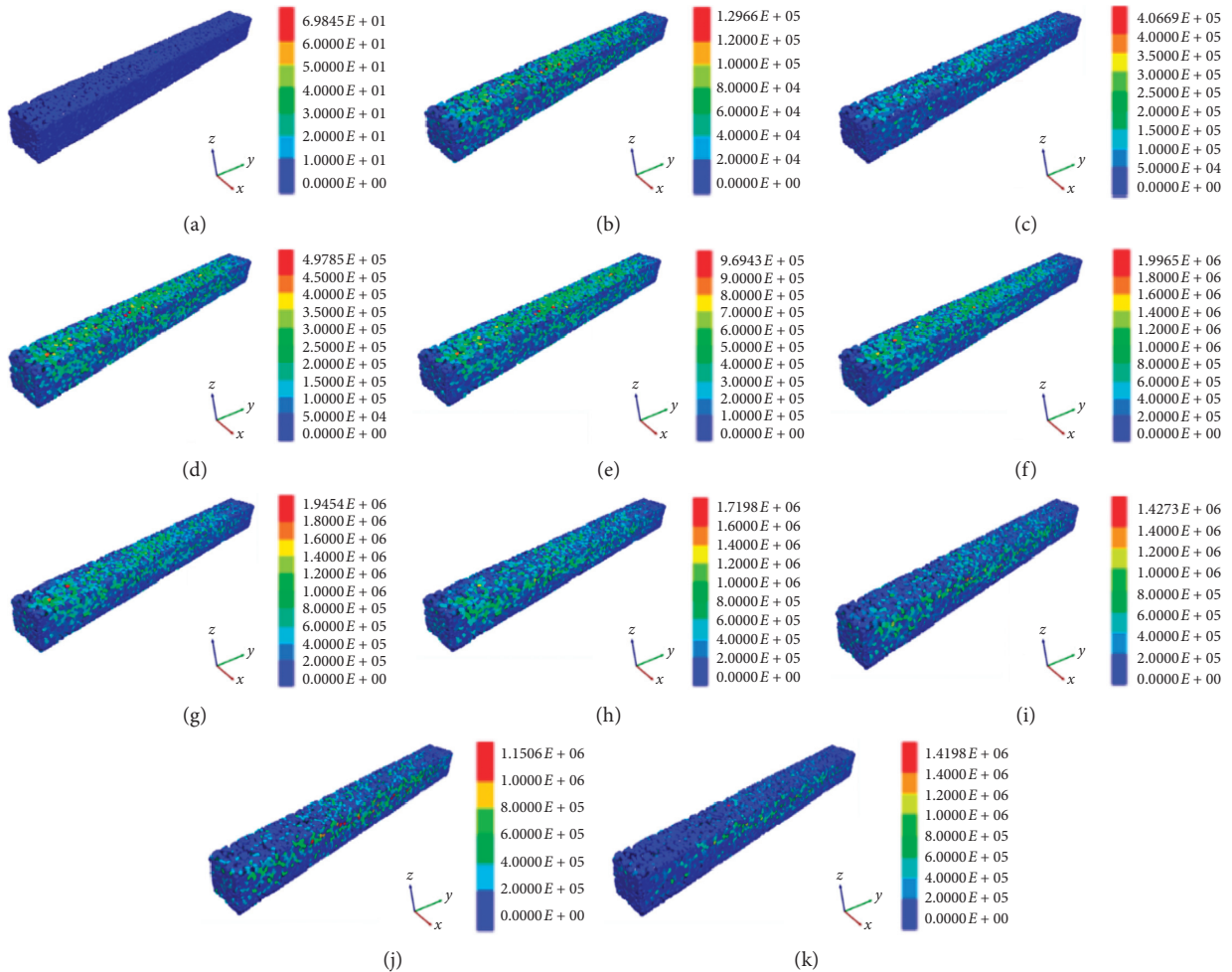FIGURE 14: z-displacement of the face floor after backfilling.

FIGURE 15: Contact force between granular coal and cross-cut with working face advancing. (a) 0 m. (b) 16 m. (c) 32 m. (d) 48 m. (e) 64 m. (f) 80 m. (g) 84 m. (h) 88 m. (i) 92 m. (j) 96 m. (k) 100 m.

6. Conclusions

(1) A support design method is proposed when longwall face strides across and passes through a roadway, which is consisting of a model to determine the roadway supporting range and support scheme. The model is built based on Terzaghi's principle, rock beam, and Protodjakonov's theory. The developed model was used to determine the range of the roadway needing supporting. And a segmental support scheme is introduced based on the developed model.

(2) An elastic model was developed to represent the mechanical behaviour of the crashed material in the gob. Comparing with Salamon's model, the elastic model provided more efficient computation and better results when the vertical stress below 20 MPa. The elastic model will be used in follow-up studies as a reference.

(3) Based on a real case, the rationality of this model was validated using a FDEM method. The results indicate that this backfilling design can meet the production requirements and is likely to significantly reduce the support cost. The results suggest that the proposed model can be used for determining the minimal thickness of the rock strata, with the error rate ranging from -10.44% to 9.97%. The results of this study are likely to be useful as a reference for the safe and efficient mining of coal resources under similar conditions.

Data Availability

Some or all data, models, or codes that support the findings of this study are available from the corresponding author upon reasonable request.

Conflicts of Interest

The authors declare no conflicts of interest.

Acknowledgments

References

[1] C. Liu, Z. Yang, P. Gong et al., "Accident analysis in relation to main roof structure when longwall face advances toward a roadway: a case study," *Advances in Civil Engineering*, vol. 2018, Article ID 3810315, 11 pages, 2018.

[2] D. C. Oyler, C. Mark, D. R. Dolinar, and R. C. Frith, "A study of the ground control effects of mining longwall faces into open or backfilled entries," *Geotechnical and Geological Engineering*, vol. 19, no. 2, pp. 137–168, 2001.

[3] W. D. Pan, G. D. Liu, and L. K. Wei, "Safety rock stratum thickness and reinforced support technology during mining face striding crosscuts," *Journal of China Coal Society*, vol. 38, no. 4, 2013.

[4] D.-Z. Kong, Z.-B. Cheng, and S.-S. Zheng, "Study on the failure mechanism and stability control measures in a large-cutting-height coal mining face with a deep-buried seam," *Bulletin of Engineering Geology and the Environment*, vol. 78, no. 8, pp. 6143–6157, 2019.

[5] Y. Lu and L. Wang, "Numerical simulation of mining-induced fracture evolution and water flow in coal seam floor above a confined aquifer," *Computers and Geotechnics*, vol. 67, pp. 157–171, 2015.

[6] M. Chen, S.-Q. Yang, Y.-C. Zhang, and C.-W. Zang, "Analysis of the failure mechanism and support technology for the Dongtan deep coal roadway," *Geomechanics and Engineering*, vol. 11, no. 3, pp. 401–420, 2016.

[7] W. Zheng, Q. Bu, and Y. Hu, "Plastic failure analysis of roadway floor surrounding rocks based on unified strength theory," *Advances in Civil Engineering*, vol. 2018, Article ID 7475698, 10 pages, 2018.

[8] H. Kang, H. Lv, X. Zhang, F. Gao, Z. Wu, and Z. Wang, "Evaluation of the ground response of a pre-driven longwall recovery room supported by concrete cribs," *Rock Mechanics and Rock Engineering*, vol. 49, no. 3, pp. 1025–1040, 2016.

[9] W. Pan, X. Nie, and X. Li, "Effect of premining on hard roof distress behavior: a case study," *Rock Mechanics and Rock Engineering*, vol. 52, no. 6, pp. 1871–1885, 2019.

[10] K. Terzaghi, *Theoretical Soil Mechanics*, John Wiley & Sons, Inc., vol. 1, Hoboken, NJ, USA, 1943.

[11] S. Mahdevari, K. Shahriar, M. Sharifzadeh, and D. D. Tannant, "Stability prediction of gate roadways in longwall mining using artificial neural networks," *Neural Computing and Applications*, vol. 28, no. 11, pp. 3537–3555, 2017.

[12] R. Šňupárek and P. Konečný, "Stability of roadways in coalmines alias rock mechanics in practice," *Journal of Rock Mechanics and Geotechnical Engineering*, vol. 2, no. 3, pp. 281–288, 2010.

[13] Q. Chang, J. Chen, H. Zhou, and J. Bai, "Implementation of paste backfill mining technology in Chinese coal mines," *The Entific World Journal*, vol. 2014, Article ID 821025, 8 pages, 2014.

[14] L. Fan and S. Liu, "Numerical prediction of in situ horizontal stress evolution in coalbed methane reservoirs by considering both poroelastic and sorption induced strain effects," *International Journal of Rock Mechanics and Mining Sciences*, vol. 104, pp. 156–164, 2018.

[15] M. Cai, M. He, and D. Liu, *Rock Mechanics and Engineering*, Science Press, Beijing, China, 2002.

[16] N. Mohammad, D. J. Reddish, and L. R. Stace, "The relation between in situ and laboratory rock properties used in numerical modelling," *International Journal of Rock Mechanics and Mining Sciences*, vol. 34, no. 2, pp. 289–297, 1997.

[17] G. S. P. Singh and U. K. Singh, "A numerical modeling approach for assessment of progressive caving of strata and performance of hydraulic powered support in longwall workings," *Computers and Geotechnics*, vol. 36, no. 7, pp. 1142–1156, 2009.

[18] Z.-L. Li, X.-Q. He, L.-M. Dou, D.-Z. Song, and G.-F. Wang, "Numerical investigation of load shedding and rockburst reduction effects of top-coal caving mining in thick coal seams," *International Journal of Rock Mechanics and Mining Sciences*, vol. 110, pp. 266–278, 2018.

[19] H. Yavuz, "An estimation method for cover pressure re-establishment distance and pressure distribution in the goaf of

longwall coal mines," *International Journal of Rock Mechanics and Mining Sciences*, vol. 41, no. 2, pp. 193–205, 2004.

[20] M. Salamon, "Mechanism of caving in longwall coal mining," in *Proceedings of the 31st US Symposium on Rock Mechanics Contributions and Challenges*, pp. 161–168, Golden, CO, USA, June 1990.

[21] M. Bai, F. S. Kendorski, and D. J. Van Roosendaal, *Chinese and North American High-Extraction Underground Coal Mining Strata Behavior and Water Protection Experience and Guidelines*, West Virginia University, Morgantown, WV, USA, 1995.

[22] A. Liu, S. Liu, G. Wang, and D. Elsworth, "Predicting fugitive gas emissions from gob-to-face in longwall coal mines: coupled analytical and numerical modeling," *International Journal of Heat and Mass Transfer*, vol. 150, Article ID 119392, 2020.

[23] S. S. Peng, *Longwall Mining*, CRC Press, Boca Raton, FL, USA, 3rd edition, 2019.

[24] H. Basarir, Y. Sun, and G. Li, "Gateway stability analysis by global-local modeling approach," *International Journal of Rock Mechanics and Mining Sciences*, vol. 113, no. 1, pp. 31–40, 2019.

[25] H. Kose and Y. Cebi, "Investigation the stresses forming during production of thick coal seam," in *Proceedings of the 6th Coal Congress of Turkey*, pp. 371–383, Zonguldak, Turkey, January 1988.

[26] M. Shabanimashcool and C. C. Li, "Numerical modelling of longwall mining and stability analysis of the gates in a coal mine," *International Journal of Rock Mechanics and Mining Sciences*, vol. 51, pp. 24–34, 2012.

[27] Y. Jiang, H. Wang, S. Xue, Y. Zhao, J. Zhu, and X. Pang, "Assessment and mitigation of coal bump risk during extraction of an island longwall panel," *International Journal of Coal Geology*, vol. 95, pp. 20–33, 2012.

[28] F. E. Garcia and J. D. Bray, "Modeling the shear response of granular materials with discrete element assemblages of sphere-clusters," *Computers and Geotechnics*, vol. 106, pp. 99–107, 2019.

[29] Y. Hu, W. Li, Q. Wang, S. Liu, and Z. Wang, "Study on failure depth of coal seam floor in deep mining," *Environmental Earth Sciences*, vol. 78, no. 24, 2019.

[30] J. Wang, S. Yang, Y. Li, L. Wei, and H. Liu, "Caving mechanisms of loose top-coal in longwall top-coal caving mining method," *International Journal of Rock Mechanics and Mining Sciences*, vol. 71, pp. 160–170, 2014.

[31] L. Li and M. Aubertin, "An improved method to assess the required strength of cemented backfill in underground stopes with an open face," *International Journal of Mining Science and Technology*, vol. 24, no. 4, pp. 549–558, 2014.

[32] M. Pattonmallory, S. M. Cramer, F. W. Smith, and P. J. Pellicane, "Nonlinear material models for analysis of bolted wood connections," *Journal of Structural Engineering (ASCE)*, vol. 123, no. 8, pp. 1063–1070, 1997.